

Bremsstrahlung signatures of dark matter annihilation in the Sun

Keita Fukushima,¹ Yu Gao,² Jason Kumar,¹ and Danny Marfatia³

¹*Department of Physics & Astronomy, University of Hawai'i, Honolulu, HI 96822, USA*

²*Department of Physics, University of Oregon, Eugene, OR 97403, USA*

³*Department of Physics & Astronomy, University of Kansas, Lawrence, KS 66045, USA*

The nonrelativistic annihilation of Majorana dark matter in the Sun to a pair of light fermions is chirality-suppressed. Annihilation to 3-body final states $\ell^+ f^- V$, where $V = W, Z, \gamma$, and ℓ and f are light fermions (that may be the same), becomes dominant since bremsstrahlung relaxes the chirality suppression. We evaluate the neutrino spectra at the source, including spin and helicity dependent effects, and assess the detectability of each significant bremsstrahlung channel at IceCube/DeepCore. We also show how to combine the sensitivities to the dark matter-nucleon scattering cross section in individual channels, since typically several channels contribute in models.

I. INTRODUCTION

Dark Matter (DM) particles X can become captured and trapped at the center of the Sun and the Earth. As the DM density grows over time, the accumulated DM can annihilate and produce a neutrino flux that is observable at a detector on Earth [1]. The annihilation channels and the final state decay products are determined by details of physics beyond the Standard Model (SM).

While it is often assumed that 2-body annihilations dominate, 3-body final states can be the leading contribution in models in which the DM candidate is a Majorana fermion. Such candidates arise, for example in supersymmetric models where the lightest supersymmetric particle is a neutralino. In such models, the cross section for dark matter annihilation to light fermions is severely suppressed [2].

The wavefunction of an initial state consisting of a pair of identical fermions must be totally antisymmetric, implying either $L = S = 0$ or $L = S = 1$, where L and S are the orbital angular momentum and spin of the pair, respectively. For the latter case, the annihilation matrix element $\mathcal{M}(XX \rightarrow f\bar{f})$ is necessarily p -wave suppressed, and is thus proportional to $v \ll 1$, where v is the relative velocity of the DM particles. The s -wave initial state is CP-odd and has zero total angular momentum; if CP-violating effects are negligible, this state must annihilate to an $L = 0, S = 0$ final state. As the final state fermions $f\bar{f}$ emerge back-to-back, they must possess the same helicity. Since particles and antiparticles of the same handedness arise from different Weyl spinors, s -wave $XX \rightarrow f\bar{f}$ annihilation requires that the initial state couple to both the f_L and f_R spinors, *i.e.*, a mixed coupling to both L/R chirality. (For further elaboration of these issues see the Appendix of Ref. [3].)

While fermion mass readily provides L-R mixing, it leads to a matrix element suppressed by m_f/m_X . If the mass term is the only source of helicity mixing, the 2-body $XX \rightarrow f\bar{f}$ annihilation cross section is heavily suppressed. However, a 3-body final state containing an additional vector boson (VB) can be CP-even with vanishing total angular momentum, even if both fermions arise from the same Weyl spinor. As a result, the 3-body annihilation cross section is not suppressed by m_f^2/m_X^2 , and becomes significant despite the additional coupling factor ($\sim \alpha$).

Radiative electroweak corrections to DM annihilation were recently considered for the gamma ray [4–6], positron [7, 8] and antiproton [8–10] spectrum of the annihilations. Recently, solar DM signals from electroweak bremsstrahlung were investigated in Ref. [11]. In comparison, we consider each significant annihilation channel separately; the corresponding event rates can be summed using annihilation branching ratios which depend on the details of a specific model. We also consider DM annihilation to left-handed and right-handed fermions separately. This is important, as the shape of the neutrino injection spectrum depends significantly on the helicity of the fermions (and in particular on their decay spectra). We also numerically propagate the neutrinos through the Sun and vacuum, with oscillations, scattering and τ -regeneration fully simulated.

In Section II, we describe the model we adopt and compute the doubly differential 3-body annihilation cross sections. The injection spectra are presented in Section III, and a description of neutrino detection in Section IV. In Section V, we investigate the discovery potential of the annihilation channels individually and in combination at the IceCube/DeepCore (IC/DC) detector. We conclude in Section VI.

II. CROSS SECTIONS

Here we briefly discuss the annihilation cross section in the case of $SU(2)$ -singlet Majorana fermion dark matter X , with a Lagrangian similar to that of Ref. [12], where X couples to SM fermions f through Yukawa terms,

$$L_{\text{int}} = y_L X P_L f \eta_L + y_L^* \bar{f} P_R X \eta_L^* + y_R \bar{X} P_R f \eta_R + y_R^* \bar{f} P_L X \eta_R^*, \quad (1)$$

where the $y_{L,R}$ are Yukawa couplings, η_L is a spin-0 $SU(2)$ doublet and η_R is a spin-0 $SU(2)$ singlet. Since X is a gauge-singlet under the SM, the two-body annihilation $XX \rightarrow VV$ (where V is a vector boson) does not occur at tree level, even if kinematically allowed. In general, one may also write a mixing term $\eta_L^* \eta_R + \eta_R^* \eta_L$, whose coefficient is proportional to the Higgs vacuum expectation value. As L-R mixing lifts the suppression on $XX \rightarrow f\bar{f}$ (see, for example, [13]), we restrict our attention to cases where such terms are negligible.

Setting $y_R = 0$ without loss of generality, the leading contributions to the 2-body annihilation cross section are given by [5]

$$v\sigma_{XX \rightarrow f\bar{f}} = \mathcal{O}\left(\frac{m_f^2}{m_X^2}\right) + \left(\frac{y_L^4}{48\pi m_X^2} \frac{1+r^2}{(1+r)^4}\right) v^2 + \mathcal{O}(v^4), \quad (2)$$

where $r = m_\eta^2/m_X^2$. As expected, the first (s -wave) term is suppressed by $m_f^2/m_X^2 \ll 1$, while the second (p -wave) term is suppressed by v^2 . Note that at freeze-out $v \sim 0.2$ is not negligible, and the speed of DM particles in the solar core is much smaller than that in the galactic halo, $v \sim 10^{-3}$.

In comparison, with the emission of a VB, the cross section for $XX \rightarrow f\bar{f}V$ can be expanded as [14]

$$v\sigma_{XX \rightarrow f\bar{f}V} \sim \frac{g^2}{4\pi m_X^2} \left[\mathcal{O}\left(\frac{v^2}{r^2}\right) + \mathcal{O}\left(\frac{v^2}{r^3}\right) + \mathcal{O}\left(\frac{1}{r^4}\right) \right]. \quad (3)$$

As expected, the first two velocity-dependent (p -wave) terms are small compared to the corresponding term in the 2-body cross-section because of the extra coupling factor $g^2/4\pi$. However, the third (s -wave) term is velocity-independent and can be significant if r is not too large. In fact, for typical halo velocities, this 3-body annihilation process dominates the 2-body process for $r < \mathcal{O}(10)$ [14]. Note that the s -wave term is not suppressed by the mass insertion as the VB spin cancels the total spin of the two fermions, which can have the same chirality.

To compute the 3-body annihilation cross section, in addition to the interaction Lagrangian in Eq. (1), we need the matter-gauge boson interaction vertices. These can be derived from the Lagrangian kinetic terms (in standard notation),

$$\mathcal{L}_D = \bar{f} \left\{ i\gamma^\mu \left(\partial_\mu - ie \frac{1}{\sqrt{2} \sin^2 \theta_W} (W_\mu^+ T_+ + W_\mu^- T_-) - ie \frac{T_3 - \sin^2 \theta_W Q}{\sin \theta_W \cos \theta_W} Z_\mu - ie A_\mu Q \right) - m \right\} f,$$

and

$$\begin{aligned} \mathcal{L}_{\text{KG}} = & |\partial_\mu \eta|^2 - i \left(\partial_\mu \eta^* \left\{ e \frac{1}{\sqrt{2} \sin^2 \theta_W} (W_\mu^+ T_+ + W_\mu^- T_-) + e \frac{T_3 - \sin^2 \theta_W Q}{\sin \theta_W \cos \theta_W} Z_\mu + e A_\mu Q \right\} \eta \right. \\ & \left. - \left\{ e \frac{1}{\sqrt{2} \sin^2 \theta_W} (W_\mu^+ T_+ + W_\mu^- T_-) + e \frac{T_3 - \sin^2 \theta_W Q}{\sin \theta_W \cos \theta_W} Z_\mu + e A_\mu Q \right\} \eta^* \partial_\mu \eta \right) - m^2 |\eta|^2 \\ & + \left\{ e \frac{1}{\sqrt{2} \sin^2 \theta_W} (W_\mu^+ T_+ + W_\mu^- T_-) + e \frac{T_3 - \sin^2 \theta_W Q}{\sin \theta_W \cos \theta_W} Z_\mu + e A_\mu Q \right\}^2 |\eta|^2. \end{aligned} \quad (4)$$

The matter-gauge boson interaction terms permit the tree-level process $XX \rightarrow f\bar{f}V$ to proceed via t - or u -channel exchange of $\eta_{L,R}$, with the VB radiated from either the external legs (*i.e.*, final state radiation), or from the virtual η (referred to as internal bremsstrahlung).

The total amplitude can be written as [14]

$$i\mathcal{M} = i[(M_A + M_A^{exc}) + (M_B + M_B^{exc}) + (M_C + M_C^{exc})], \quad (5)$$

where the subscripts A-C refer to the diagrams in Fig. 1. We take the fermion masses to be negligible compared to the mass of the DM particle ($m_f/m_X \ll 1$). Using the *FeynCalc* [15] package, we find that the squared matrix element (summed over polarizations and averaged over initial spins) for annihilation to *e.g.*, $f_L \bar{f}_L Z$ is

$$|\mathcal{M}|_{XX \rightarrow f_L \bar{f}_L Z}^2 = \frac{e^2 (1 - 2 \sin^2 \theta_W)^2 |y_L|^4 (4(x_1 + x_2 - 1) + \frac{m_Z^2}{m_X^2}) \left(2(x_1^2 - 2x_1 + x_2^2 - 2x_2 + 2) - \frac{m_Z^2}{m_X^2} \right)}{8 \sin^2 \theta_W \cos^2 \theta_W m_X^2 (1 - 2x_1 - r)^2 (1 - 2x_2 - r)^2}, \quad (6)$$

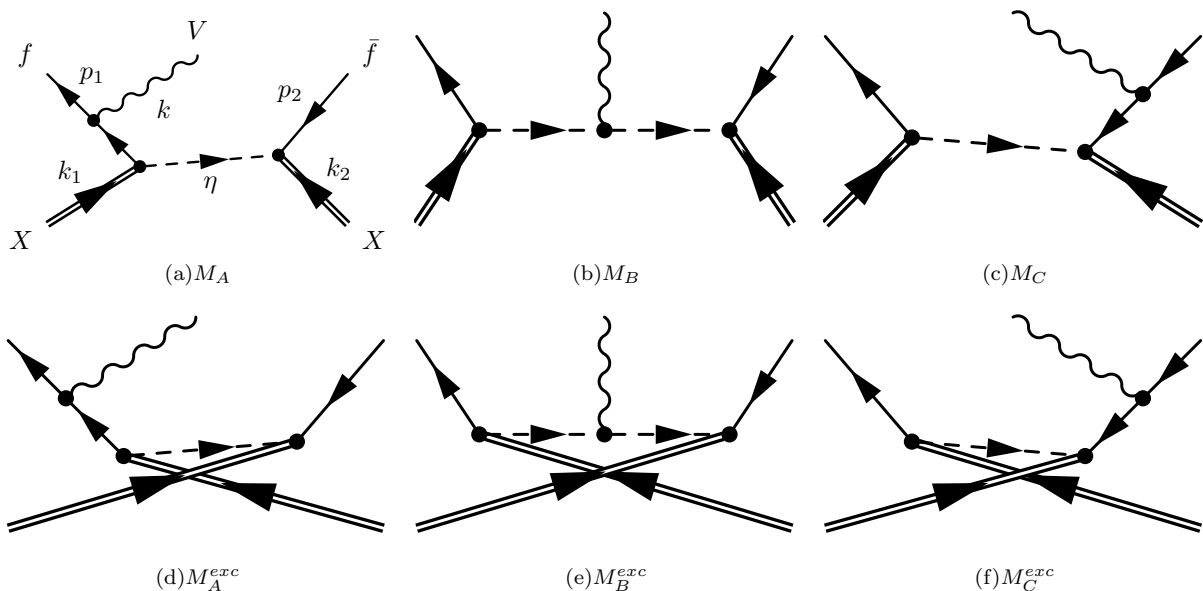


FIG. 1. Feynman diagrams for the 3-body annihilation process, $XX \rightarrow f\bar{f}V$. The incoming DM particles X have momenta k_1 and k_2 . f, \bar{f} are the outgoing fermion and antifermion with momenta p_1 and p_2 , respectively. η is the mediator particle, and V is a gauge boson (γ, Z , or W) with momentum k .

where we use the notation of Ref. [6] and define $x_1 = E_{f_1}/m_X$, $x_2 = E_{f_2}/m_X$ and $x_3 = E_Z/m_X$, in the static center of mass frame with $x_1 + x_2 + x_3 = 2$.

We separately compute the annihilation cross section to final states with any choice of fermion helicities. The differential cross sections,

$$v_{rel} \frac{d\sigma}{dx_1 dx_2} = \frac{|\mathcal{M}|^2}{128\pi^3}, \quad (7)$$

(where $v_{rel} = v_1 - v_2$), for all final state channels and helicities are given in Appendix A; our results agree with those in Refs. [4, 6, 10, 14]. We have checked that integrating the differential cross sections in the $m_Z \rightarrow 0$ limit, yields the results in Refs. [5, 7, 9, 14]. An analytic expression for the total cross section is given in Ref. [5].

III. NEUTRINO SPECTRA

In this section we discuss neutrino injection from the leading annihilation channels with VB-bremsstrahlung. We focus on the couplings of DM to leptons because these are the most relevant to searches at neutrino detectors. In particular, lepton couplings produce neutrinos directly as part of the 3-body final state, and can provide a substantial contribution to the neutrino spectrum at high energy. However, lepton couplings do not contribute significantly to the DM capture rate; although DM can scatter off electrons in the Sun, such collisions do not result in DM capture because the momentum transfer is very small (since $m_e \ll m_X$). Additional interactions between DM and light quarks thus provide the dominant contribution to the capture rate. It is worth noting that, although DM-quark interactions can also induce annihilation, these are unlikely to produce energetic neutrinos. These annihilation processes do not directly produce neutrinos in either the 2-body or 3-body final state, and the outgoing light quarks hadronize and stop before decaying, resulting in a very soft neutrino spectrum. Henceforth, we simply assume that there are some additional DM-quark interactions responsible for DM capture in the Sun.

In general, the different annihilation channels are not independent of each other, and their branching fractions are determined by the couplings $y_{L,R}$ (assuming the $\eta_{L,R}$ states have degenerate mass). We present the spectra for individual channels, however, in order to illustrate which channels provide the hardest neutrino spectra. Moreover, for models in which the degeneracy of the $\eta_{L,R}$ is broken, the total injection spectrum can be found by summing the spectra of the individual channels after an appropriate rescaling.

Lepton chirality plays an important role for both the annihilation cross section and the shape of neutrino spectrum arising from lepton decays. We investigate a scenario of flavor-independent lepton couplings, and a pure third-generation coupling (100% τ) scenario.

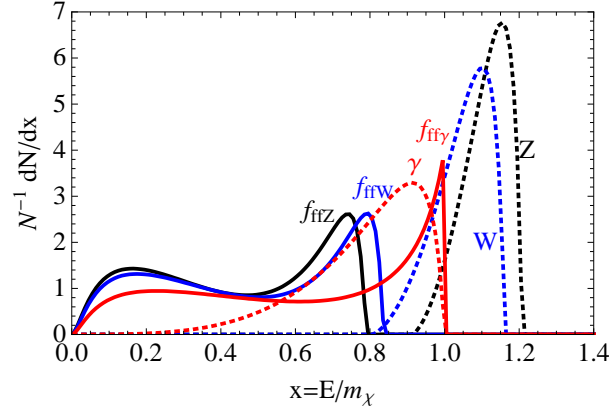


FIG. 2. Normalized fermion spectra (solid) and VB spectra (dotted) for $XX \rightarrow f\bar{f}V$ for $m_X = 100$ GeV and $m_\eta = 105$ GeV from Eq. (8). For light DM, off-shell VB emission is significant, resulting in 4-body spectra that deviate from these on-shell calculations.

We calculate the tree-level matrix element for the 4-body annihilation, $XX \rightarrow f\bar{f}(V \rightarrow f\bar{f})$ for all choices of fermion helicity. Thus, contributions in which the gauge boson is produced off-shell are included. The SM quantum numbers of $\eta_{L,R}$ are determined by gauge-invariance, and we assume that all scalar partners $\eta_{L,R}$ share a universal mass $m_\eta = \sqrt{r}m_X$. Consequently, the matrix elements are entirely determined by $y_{L,R}$, r and m_X .

The leading contributors to the neutrino spectrum are

- Primary neutrinos produced directly from the annihilation ($XX \rightarrow \nu\bar{\nu}Z, l^-\bar{\nu}W^+, l^+\nu W^-$).
- Secondary neutrinos produced from the decay of primary $W^\pm \rightarrow l^\pm\nu, Z \rightarrow \nu\bar{\nu}$ produced in the annihilation ($XX \rightarrow \nu\bar{\nu}Z, l^+l^-Z, l^-\bar{\nu}W^+, l^+\nu W^-$).
- Neutrinos from the decay of primary $\tau/\bar{\tau}$'s produced in the annihilation process ($XX \rightarrow \bar{\tau}\tau(Z, \gamma), \bar{\nu}_\tau\tau W^+, \bar{\tau}\nu_\tau W^-$).

We study the following channels:

- (1) $XX \rightarrow \tau_L\bar{\tau}_L\gamma$
- (2) $XX \rightarrow \tau_R\bar{\tau}_R\gamma$
- (3) $XX \rightarrow \nu\bar{\nu}(Z \rightarrow \nu\bar{\nu})$ for $\nu_e : \nu_\mu : \nu_\tau = 1 : 1 : 1$
- (4) $XX \rightarrow \nu_\tau\bar{\nu}_\tau(Z \rightarrow \nu\bar{\nu})$ (100% $\nu_\tau\bar{\nu}_\tau Z$)
- (5) $XX \rightarrow \tau_L\bar{\tau}_L(Z \rightarrow \nu\bar{\nu})$
- (6) $XX \rightarrow \tau_R\bar{\tau}_R(Z \rightarrow \nu\bar{\nu})$
- (7) $XX \rightarrow \bar{\tau}_L\nu_\tau(W^- \rightarrow l^-\bar{\nu}_l) + c.c$
- (8) $XX \rightarrow \bar{l}_L\nu(W^- \rightarrow l^-\bar{\nu}_l) + c.c$ for $\nu_e : \nu_\mu : \nu_\tau = 1 : 1 : 1$
- (9) $XX \rightarrow l^+l^-(Z \rightarrow \nu\bar{\nu}, \bar{\tau}\tau), l = e, \mu$

The subscripts L, R refer to the helicity of the Weyl spinor (*e.g.*, $\bar{\tau}_L$ is the antiparticle of a left-handed τ^- , which is a right-handed τ^+), and ‘c.c.’ denotes the CP conjugate process. In addition to the three sources of neutrinos described above, for channel (9) we also include tertiary neutrinos arising from the decay of secondary τ 's produced from primary Z decay. This is the only channel for which the tertiary contribution is significant.

Since the dense solar medium readily absorbs electrons and muons, channels (1-2) are the only channels with photon-bremsstrahlung that yield a significant neutrino flux. In these channels neutrinos arise from τ decay, so the neutrino injection spectra are rather soft and are dominated by the ν_τ flavor. Also, since the photon does not decay, the primary lepton and VB spectra can be obtained from the doubly-differential 3-body ($XX \rightarrow f\bar{f}V$) annihilation cross section,

$$\frac{d\sigma}{dx_1} = \int_{x_2^-}^{x_2^+} dx_2 \frac{d\sigma}{dx_1 dx_2}, \quad \frac{d\sigma}{dx_V} = \int_{x_1^-}^{x_1^+} dx_1 \left. \frac{d\sigma}{dx_1 dx_2} \right|_{x_2=2-x_1-x_V}, \quad (8)$$

where $x_1^\pm = \frac{1}{2}(2 - x_V \pm \sqrt{x_V^2 - r_V})$, $x_2^- = 1 - x_1 - r_V/4$, $x_2^+ = 1 - r_V/(4(1 - x_1))$, and $r_V \equiv (m_V/m_X)^2$. The lepton and VB spectra are plotted in Fig. 2 for $m_X = 100$ GeV and $m_\eta = 105$ GeV.

Channels (3-6) involve Z -strahlung. Primary $\nu\bar{\nu}$ are produced in channels (3-4), and provide the dominant contribution to the neutrino spectrum. Channels (5-6) lead to softer spectra because the primary fermions are τ leptons. The

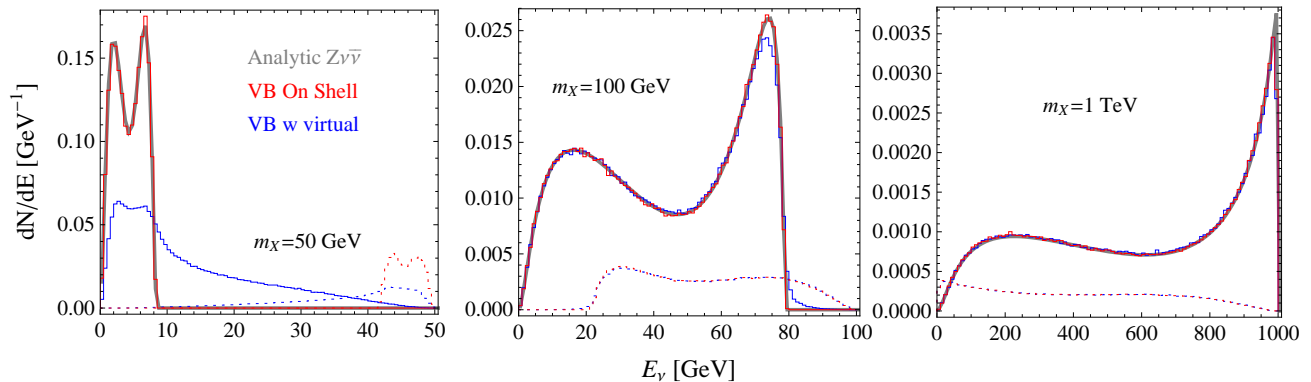


FIG. 3. Modification of the spectra from virtual VB production in the $XX \rightarrow \nu\bar{\nu}Z$ channel for $m_X = 50, 100$ and 1000 GeV. The primary (solid) and secondary (dotted) neutrino spectra are shown. The ‘On Shell’ and ‘w(ith) virtual’ curves are generated using *CalcHep*. Spectra obtained from Eqs. (A1) and (8) are also shown.

case of Z -strahlung in which the primary fermions are e/μ yields a still softer neutrino spectrum, and is treated separately in Channel (9). Channels (7-8) involve W -bremsstrahlung (with either 100% ν_τ or flavor-independent couplings), in which both primary and secondary neutrinos and charged leptons appear. The coupling in W -bremsstrahlung is solely left-handed. We only consider leptonic W/Z decays, as the hadronic decays suffer from absorption in the solar medium and produce considerably softer neutrinos.

To incorporate virtual W/Z contributions in Channels (3-9), we use the numerical package *CalcHep* [16] to compute the primary and secondary fermion spectra separately, and apply helicity-dependent decay to the τ leptons, if present. In Fig. 3, we show the primary and secondary neutrino spectra from $XX \rightarrow \nu\bar{\nu}Z$ for $m_X = 50, 100, 1000$ GeV, assuming either an on-shell VB, or allowing the VB to be off-shell. For DM mass above 100 GeV, the virtual contribution becomes subdominant and the primary spectra are reasonably well-described by 3-body cross sections.

We display the neutrino injection spectrum from each channel for $m_X = 100$ GeV, $m_\eta = 105$ GeV (Fig. 4), and for $m_X = 1000$ GeV, $m_\eta = 1050$ GeV (Fig. 5). The antineutrino injection spectra are identical.

Although the 3-body differential cross section for $XX \rightarrow \tau_R\bar{\tau}_R V$ can be obtained from that of $XX \rightarrow \tau_L\bar{\tau}_L V$ by simply rescaling by coupling factors (see Appendix A), the resulting neutrino spectra are quite different. This can be seen by comparing the spectra for Channels (1) and (2), and for Channels (5) and (6) in Figs. 4 and 5. The reason for this difference is that the neutrino spectrum arising from the decay of a τ depends on its helicity; the neutrino spectrum arising from a highly-boosted left-handed τ differs markedly from that of a right-handed τ . For each channel, the fraction of left/right handed τ is set by the couplings. W decay produces 100% left-handed τ while the left/right fraction from Z decay is 57%/43%. See Ref. [17] for a description of our treatment. Note that the channels dominated by τ decay lead to a rather soft neutrino spectrum; its power-law shape is less distinctive compared to channels that yield primary neutrinos.

Due to the finite mass of the W/Z bosons, the neutrino spectra depend non-trivially on m_X . Consider, for example, the $XX \rightarrow \nu\bar{\nu}Z$ channel: if $m_X \sim m_Z/2$, then the cross section for producing an on-shell Z is suppressed by the phase space of the ‘primary’ neutrinos ($E_\nu \sim m_X - m_Z/2$). The primary neutrino can be much softer than m_X , even below that of the secondary neutrinos, as shown in Fig. 3. As can be seen from Fig. 5, for $m_X \gg m_Z$, the $\nu\bar{\nu}Z$ and $l\nu W$ channels are by far the hardest.

It is worth noting, however, that the finite mass of the the W and Z gauge bosons can also enhance the annihilation cross section to those channels. The reason for this enhancement is that for some regions of phase space, the final state can only have vanishing total angular momentum if the gauge boson is helicity-0. These contributions must vanish in the $m_V \rightarrow 0$ limit, implying that these terms in the squared matrix element scale as m_V^2/m_X^2 .

The mediator mass m_η also has a noticeable impact on the shape of neutrino spectrum. In general a larger m_η leads to a neutrino energy distribution that is less peaked at the end-point; this effect could slightly enhance the signal rate, since at lower energy (yet above detector thresholds) neutrinos suffer less attenuation from scattering. However, for the values of m_X under consideration, varying m_η yields only insignificant changes to the shape of the spectrum. Moreover, the annihilation cross section is suppressed by $1/r^2$. We use a low mediator mass $r = 1.1$ throughout.

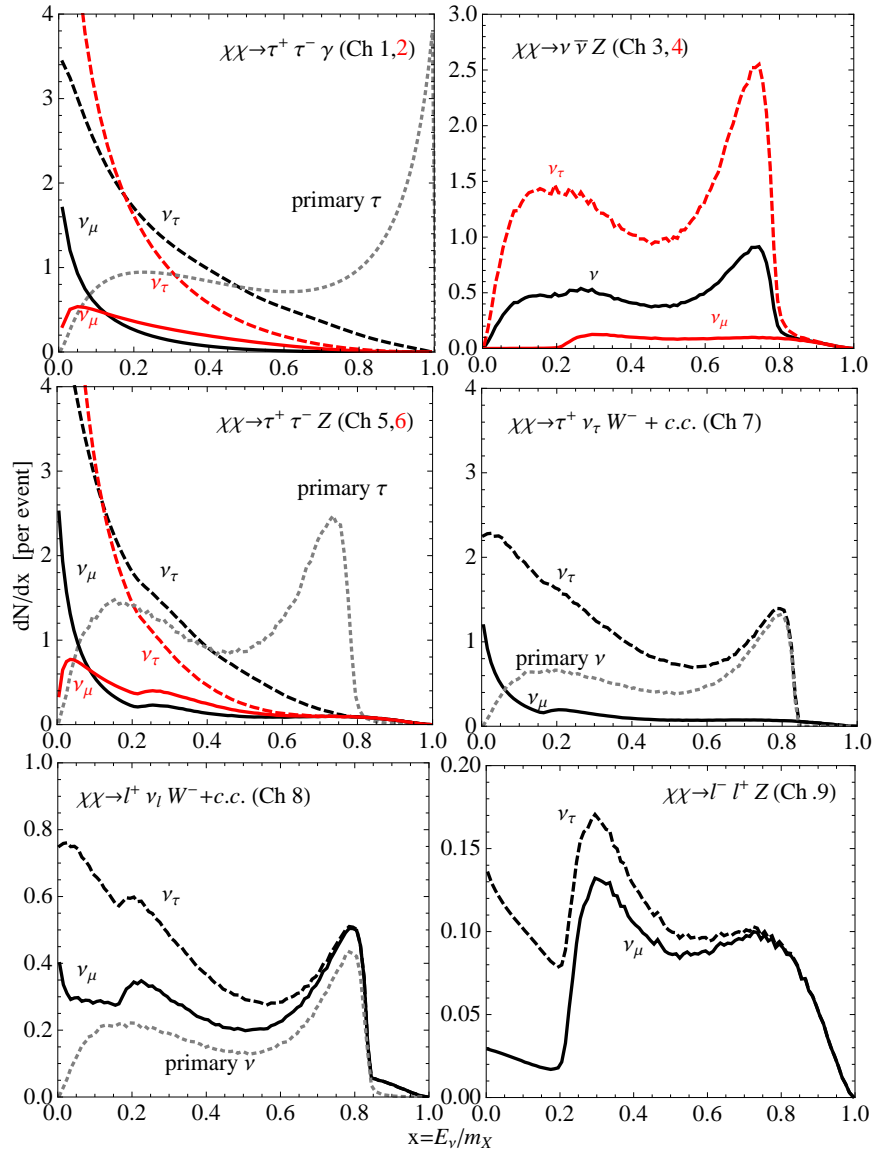


FIG. 4. ν_μ and ν_τ injection spectra from each annihilation channel (as labeled), including τ decay contributions, for $m_X = 100$ GeV and $m_\eta = 105$ GeV. The ν_e injection spectra are identical to that of ν_μ . For comparison, the gray dotted curves show the primary lepton spectrum in each case. The antineutrino injection spectra are identical.

IV. NEUTRINO DETECTION

After injection at the solar center, the neutrinos propagate through the Sun, and then through vacuum to Earth. In doing so, they oscillate and undergo scattering. We take the neutrino mixing parameters to be

$$\delta m_{21}^2 = 8.1 \times 10^{-5} \text{ eV}^2, \quad \delta m_{31}^2 = 2.2 \times 10^{-3} \text{ eV}^2, \quad \theta_{12} = 33.2^\circ, \quad \theta_{23} = 45^\circ, \quad \theta_{13} = 8.8^\circ,$$

where $\delta m_{ji}^2 = m_j^2 - m_i^2$ and we use the value of θ_{13} recently measured by the Daya Bay experiment [18]. For details of our simulation of neutrino propagation (including oscillations, tau-regeneration, and energy losses due to collisions), and muon detection at IceCube/Deepcore, see Refs. [17, 19].

To assess the IC/DC sensitivity we choose a muon energy window, $E_{th} \leq E_\mu \leq m_X$, where E_{th} is the detector threshold. We target a 3σ detection, $N^{sig} = 3\sqrt{N^{atm}}$, where N^{sig} and N^{atm} are the number of signal and atmospheric background events,

$$N^{sig} = \int dt \int_{E_{th}}^{m_X} \mathcal{V}(\theta(t), E_\mu) \frac{d\Phi^{sig}}{dE_\mu} dE_\mu, \quad (9)$$

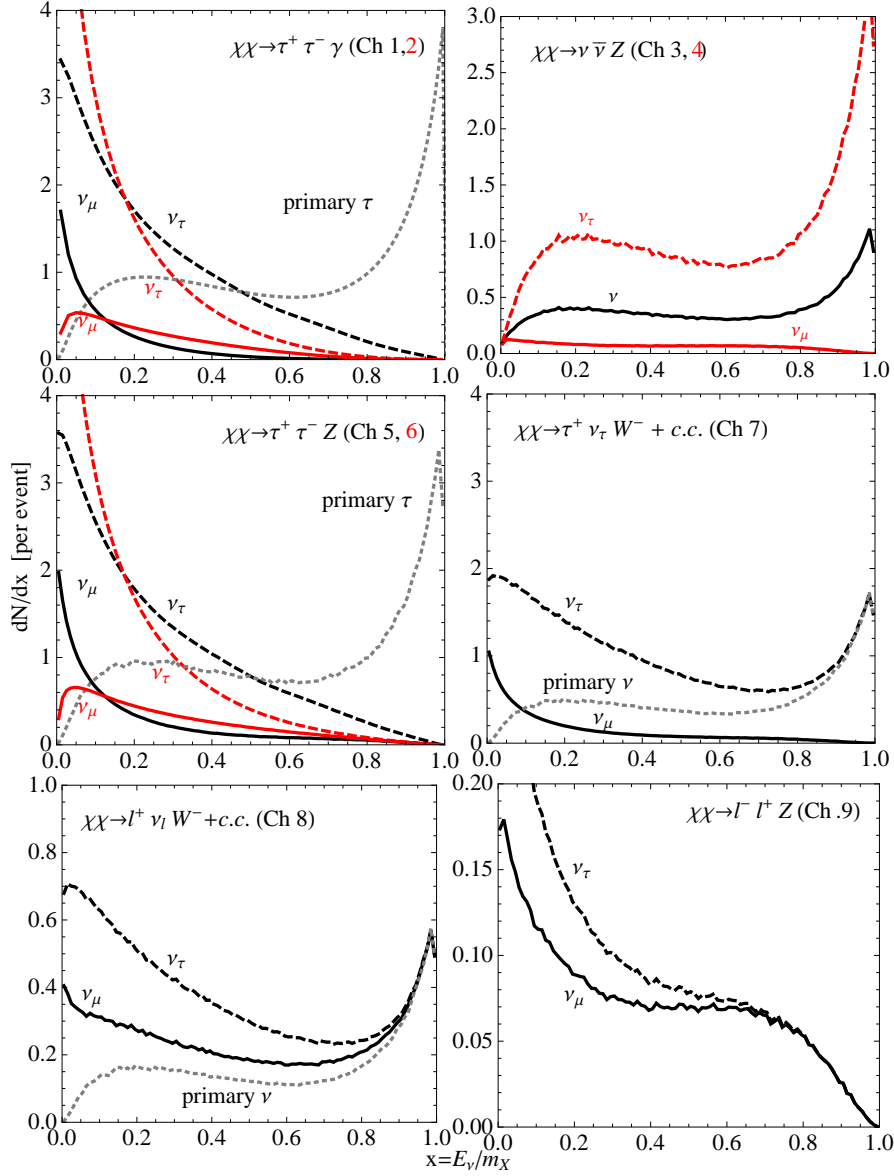


FIG. 5. Similar to Fig. 4, for $m_X = 1000$ GeV and $m_\eta = 1050$ GeV.

$$N^{atm} = \pi \delta_\theta^2 \int dt \int_{E_{th}}^{m_X} \mathcal{V}(\theta(t), E_\mu) \frac{d\Phi(\theta(t))^{atm}}{dE_\mu d\Omega} dE_\mu. \quad (10)$$

Here, Φ^{sig} and Φ^{atm} are the muon fluxes generated by the signal and atmospheric neutrinos incident on ice, respectively, and \mathcal{V} is the effective dimension of the IC/DC detector relevant to the event type. For neutrinos arriving from the direction of the Sun, most charged leptons scatter within a cone of half-angle,

$$\delta_\theta = 20^\circ \sqrt{\frac{10 \text{ GeV}}{m_X}}; \quad (11)$$

see, *e.g.*, [20]. Equation (11) gives the intrinsic scattering angle for incoming neutrinos with energy $\sim m_X$, which is comparable to the IC detector's angular resolution, and which we use to estimate the atmospheric background. Note that since N^{atm} scales quadratically with δ_θ , the constraint on the DM annihilation rate scales linearly with δ_θ .

Besides the variation with zenith angle and event energy, \mathcal{V} depends on whether the muon event is *up-going* or *contained* [21]. Up-going (contained) events refer to upward going muon tracks that start outside (inside) the instrumented volume of the detector. A discussion of the effective detector dimensions for these two types of events can be found in Refs. [17, 21]. In this analysis we consider up-going muon events for IC and contained events for

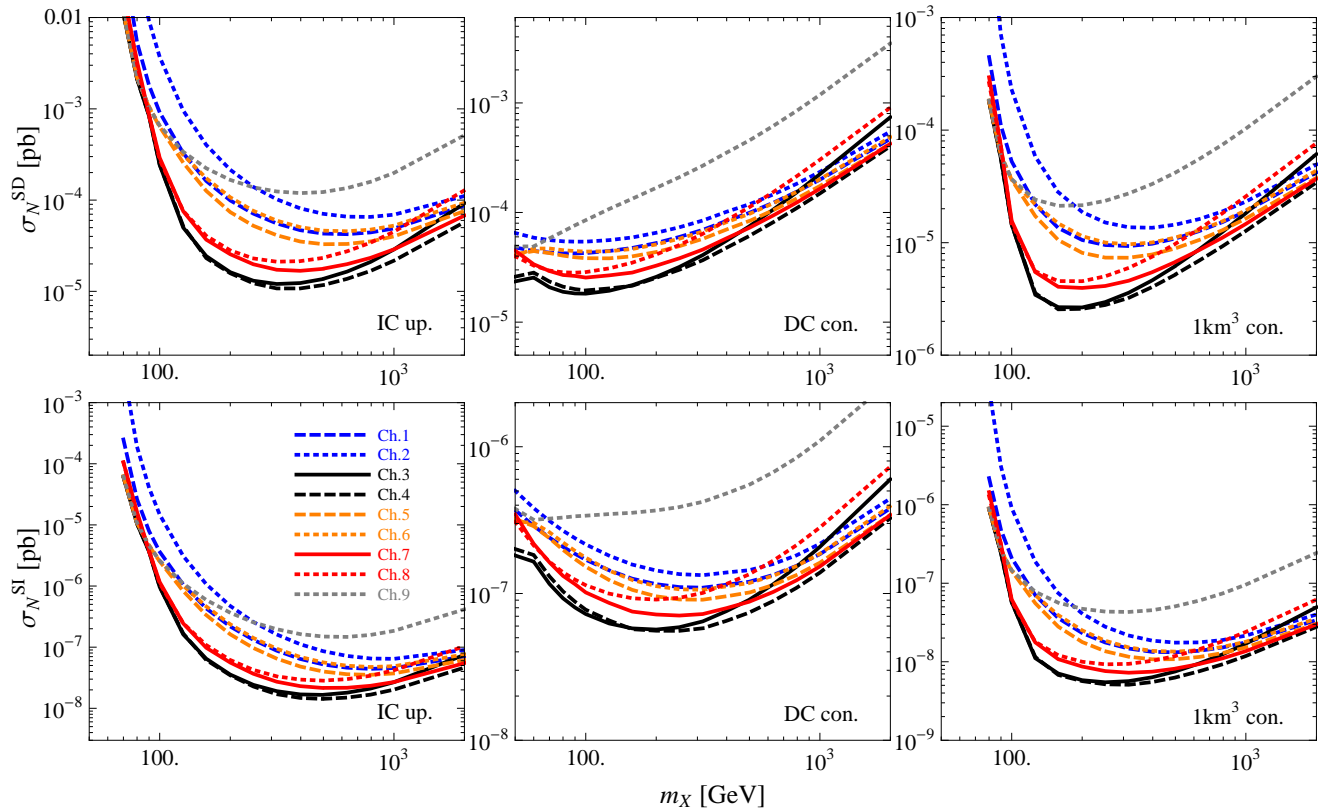


FIG. 6. The 3σ sensitivity to σ_N^{SD} and σ_N^{SI} of IC up-going, IC contained, and DC contained events, with one year of data. We assume that the DM capture and annihilation processes are in equilibrium, and set the branching fraction to each channel equal to unity.

DC, and a 1 km^3 effective volume with a 70 GeV energy threshold as an estimate for IC contained events. The effective IC area for up-going events falls rapidly below $E_{th} = 60$ GeV and we assume $E_{th} = 10$ GeV for the DC subdetector. Since observations track the trajectory of the Sun, we use the zenith-angle dependent atmospheric ν_μ flux measured by Super-Kamiokande [22]. The DM-induced muon flux has an energy spectrum that is determined by the DM capture rate and the neutrino spectrum. The time integral in Eqs. (9-10) spans half a year for IC and a full year for DC, which has 4π angular coverage. Descriptions of our calculations of up-going and contained event rates are provided in Refs. [17, 19].

V. DISCOVERY POTENTIAL

IceCube's 3σ sensitivity to DM annihilation can be determined by setting $N^{sig} = 3\sqrt{N^{atm}}$. We assume that the DM capture and annihilation processes in the Sun are in equilibrium,¹ in which case a constraint on the annihilation rate can be directly translated into a constraint on $\sigma_N \times BF_j$, the product of the DM-nucleon scattering cross section and the branching fraction to the annihilation channel in question. We normalize the branching fraction to leptonic channels $BF(\text{leptons})$ to unity, so that $\sum_j BF_j = BF(\text{leptons}) = 1$. Therefore, the sensitivities to the DM-nucleon cross section presented below should be divided by the actual value of $BF(\text{leptons})$. In Table I, we present the sensitivity to each annihilation channel (using each of the three event samples) for $m_X = 50, 100$ GeV and 1 TeV. The 3σ sensitivity to the cross section for spin-independent (SI) and spin-dependent (SD) scattering are listed separately as

¹ Whether dark matter capture and annihilation are in equilibrium is very model dependent. We pick the equilibrium case as a reference signal rate and present the rest of the calculation in as model-independent a manner as possible. Given the details of a specific model, the total annihilation rate (as a fraction of the capture rate) and the annihilation branching fractions can be determined, and our results can be translated into a bound on the particular model.

Note that for $r = 1.1$, $y_L = y_R = 1$ and $m_X = 100$ GeV, the total annihilation cross section to leptonic final states is 2.4 pb, and for $y_L = y_R = \sqrt{4\pi}$ and $m_X = 1000$ GeV it is 0.8 pb. For annihilation cross sections of this order, and for scattering cross sections of the size to which IC/DC is sensitive, equilibrium will hold. There can also be a contribution to the total annihilation cross section from quark final states (which provide only a subleading contribution to the neutrino spectrum).

		combined (pb)		IC up.			DC con.			1km ³ con. ($E_\mu > 70$ GeV)		
m_X (GeV), δ_θ	Ch.#	σ_N^{SD}	σ_N^{SI}	σ_N^{SD}	σ_N^{SI}	N^{atm}	σ_N^{SD}	σ_N^{SI}	N^{atm}	σ_N^{SD}	σ_N^{SI}	N^{atm}
$m_X = 50$ $\delta_\theta = 8.9^\circ$	1	4.8×10^{-5}	3.7×10^{-7}				4.8×10^{-5}	3.7×10^{-7}				
	2	6.5×10^{-5}	5.0×10^{-7}				6.5×10^{-5}	5.0×10^{-7}				
	3	2.4×10^{-5}	1.8×10^{-7}				2.4×10^{-5}	1.8×10^{-7}				
	4	2.6×10^{-5}	2.0×10^{-7}				2.6×10^{-5}	2.0×10^{-7}				
	5	4.2×10^{-5}	3.2×10^{-7}				4.2×10^{-5}	3.2×10^{-7}	4.7×10^2			
	6	4.0×10^{-5}	3.1×10^{-7}				4.0×10^{-5}	3.1×10^{-7}				
	7	4.5×10^{-5}	3.5×10^{-7}				4.5×10^{-5}	3.5×10^{-7}				
	8	4.9×10^{-5}	3.8×10^{-7}				4.9×10^{-5}	3.8×10^{-7}				
	9	4.0×10^{-5}	3.1×10^{-7}				4.0×10^{-5}	3.1×10^{-7}				
$m_X = 100$ $\delta_\theta = 6.3^\circ$	1	3.3×10^{-5}	1.3×10^{-7}	9.1×10^{-4}	3.6×10^{-6}		4.3×10^{-5}	1.7×10^{-7}		5.3×10^{-5}	2.1×10^{-7}	
	2	5.3×10^{-5}	2.1×10^{-7}	3.7×10^{-3}	1.5×10^{-5}		5.4×10^{-5}	2.2×10^{-7}		2.3×10^{-4}	9.1×10^{-7}	
	3	1.1×10^{-5}	4.5×10^{-8}	2.4×10^{-4}	9.6×10^{-7}		1.8×10^{-5}	7.2×10^{-8}		1.4×10^{-5}	5.8×10^{-8}	
	4	1.2×10^{-5}	4.6×10^{-8}	2.5×10^{-4}	9.8×10^{-7}		2.0×10^{-5}	7.8×10^{-8}		1.4×10^{-5}	5.7×10^{-8}	
	5	2.6×10^{-5}	1.0×10^{-7}	6.4×10^{-4}	2.5×10^{-6}	24	3.8×10^{-5}	1.5×10^{-7}	2.7×10^2	3.6×10^{-5}	1.4×10^{-7}	2.8×10^2
	6	2.8×10^{-5}	1.1×10^{-7}	6.5×10^{-4}	2.6×10^{-6}		4.4×10^{-5}	1.8×10^{-7}		3.6×10^{-5}	1.4×10^{-7}	
	7	1.3×10^{-5}	5.3×10^{-8}	2.9×10^{-4}	1.2×10^{-6}		2.6×10^{-5}	1.0×10^{-7}		1.6×10^{-5}	6.2×10^{-8}	
	8	3.4×10^{-5}	1.3×10^{-7}	6.5×10^{-4}	2.6×10^{-6}		8.5×10^{-5}	3.4×10^{-7}		3.7×10^{-5}	1.5×10^{-7}	
	9	1.3×10^{-5}	5.2×10^{-8}	2.8×10^{-4}	1.1×10^{-6}		2.9×10^{-5}	1.1×10^{-7}		1.5×10^{-5}	5.9×10^{-8}	
$m_X = 1000$ $\delta_\theta = 2^\circ$	1	1.8×10^{-5}	1.6×10^{-8}	4.9×10^{-5}	4.5×10^{-8}		2.0×10^{-4}	1.9×10^{-7}		1.9×10^{-5}	1.8×10^{-8}	
	2	2.2×10^{-5}	2.0×10^{-8}	6.9×10^{-5}	6.4×10^{-8}		2.3×10^{-4}	2.2×10^{-7}		2.3×10^{-5}	2.1×10^{-8}	
	3	1.5×10^{-5}	1.4×10^{-8}	2.9×10^{-5}	2.7×10^{-8}		2.2×10^{-4}	2.1×10^{-7}		1.8×10^{-5}	1.7×10^{-8}	
	4	1.1×10^{-5}	1.0×10^{-8}	2.2×10^{-5}	2.0×10^{-8}		1.5×10^{-4}	1.4×10^{-7}		1.3×10^{-5}	1.2×10^{-8}	
	5	1.5×10^{-5}	1.4×10^{-8}	4.0×10^{-5}	3.7×10^{-8}	20	1.7×10^{-4}	1.6×10^{-7}	30	1.6×10^{-5}	1.5×10^{-8}	82
	6	1.8×10^{-5}	1.7×10^{-8}	5.2×10^{-5}	4.9×10^{-8}		2.0×10^{-4}	1.9×10^{-7}		1.9×10^{-5}	1.8×10^{-8}	
	7	1.3×10^{-5}	1.2×10^{-8}	2.9×10^{-5}	2.7×10^{-8}		1.6×10^{-4}	1.5×10^{-7}		1.5×10^{-5}	1.4×10^{-8}	
	8	9.1×10^{-5}	8.5×10^{-8}	2.0×10^{-4}	1.8×10^{-7}		1.2×10^{-3}	1.1×10^{-6}		1.0×10^{-4}	9.6×10^{-8}	
	9	2.2×10^{-5}	2.1×10^{-8}	4.5×10^{-5}	4.2×10^{-8}		3.0×10^{-4}	2.8×10^{-7}		2.6×10^{-5}	2.4×10^{-8}	

TABLE I. The 3σ sensitivity to the spin-dependent (SD) and spin-independent (SI) DM-nucleon scattering cross sections for each annihilation channel with one year of data. The number of atmospheric background events N^{atm} in one year at DeepCore and 180 days at IceCube is also provided. The muon energy window runs from the experimental threshold (10 GeV for DC, 60 GeV and 70 GeV for IC up-going and contained) to m_X .

σ_N^{SI} and σ_N^{SD} , respectively. The dependence of the equilibrium annihilation rate on σ_N is calculated using the method described in Ref. [20]. The corresponding background rates are also listed. In Fig. 6, we plot the 3σ sensitivity to the DM-nucleon scattering cross section (setting the branching fraction to each channel equal to 1), under the assumption that equilibrium holds between capture and annihilation in each individual channel. The combined sensitivity of the

three event samples obtained from $\sqrt{\sum_{i=1}^3 \frac{(N_i^{sig})^2}{N_i^{atm}}} = 3$, is shown in Fig. 7 for each channel.

For any particular model, there will be several annihilation channels and the total event rate will be the sum of the contributions from each channel. To compute the sensitivity to the DM-nucleon cross section from a combination of channels, σ_N^{comb} , we utilize the fact that signal significance scales linearly with the cross section. We denote by $\sigma_{N,i}^j$ the 3σ sensitivity of IC/DC in annihilation Channel (j), using event sample i (either DC contained events, IC up-going events, or IC contained events), as reported in Table I. Denoting the branching fraction to Channel (j) by BF_j , we find the 3σ sensitivity for event sample i from

$$\sigma_{N,i} = \left[\sum_j \frac{BF_j}{\sigma_{N,i}^j} \right]^{-1}. \quad (12)$$

The 3σ combined sensitivity from a combination of channels and all three event types is then

$$\sigma_N^{comb} = \left[\sum_{i=1}^3 \frac{1}{\sigma_{N,i}^2} \right]^{-\frac{1}{2}}. \quad (13)$$

In Table II, we show the 3σ sensitivity to σ_N^{SD} and σ_N^{SI} for $m_X = 100, 1000$ GeV for three models: DM with couplings only to left-handed third generation leptons ($y_R = 0$), DM with couplings only to τ_R ($y_L = 0$), and DM with equal couplings to left-handed and right-handed third generation leptons ($y_L = y_R$).

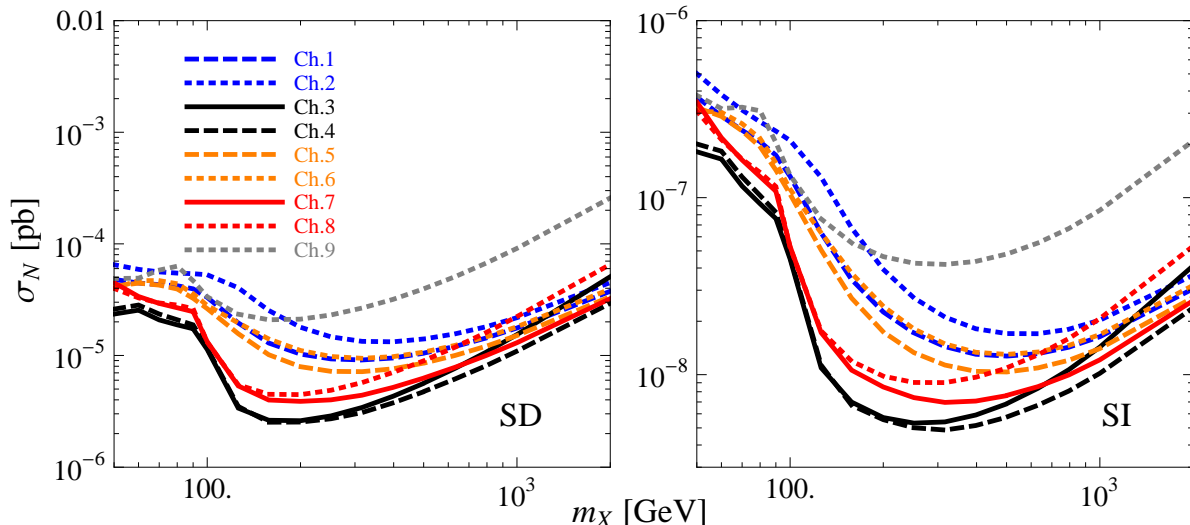


FIG. 7. The 3σ sensitivity to σ_N^{SD} and σ_N^{SI} of the combined IC up-going, IC contained, and DC contained event samples, with one year of data. In most of the mass range, contained events dominate the signal rate. DC dominates the sensitivity for m_X below the energy threshold of the less dense IC strings.

model	$\sigma_N^{SD} (m_X = 100 \text{ GeV})$	$\sigma_N^{SD} (m_X = 1 \text{ TeV})$	$\sigma_N^{SI} (m_X = 100 \text{ GeV})$	$\sigma_N^{SI} (m_X = 1 \text{ TeV})$
$y_R = 0$	$1.4 \times 10^{-5} \text{ pb}$	$1.3 \times 10^{-5} \text{ pb}$	$5.3 \times 10^{-8} \text{ pb}$	$1.2 \times 10^{-8} \text{ pb}$
$y_L = 0$	$3.4 \times 10^{-5} \text{ pb}$	$2.1 \times 10^{-5} \text{ pb}$	$1.4 \times 10^{-7} \text{ pb}$	$1.9 \times 10^{-8} \text{ pb}$
$y_L = y_R$	$1.4 \times 10^{-5} \text{ pb}$	$1.4 \times 10^{-5} \text{ pb}$	$5.6 \times 10^{-8} \text{ pb}$	$1.3 \times 10^{-8} \text{ pb}$

TABLE II. The 3σ sensitivity to σ_N^{SD} and σ_N^{SI} (with 1 year of data) for three models with Yukawa couplings only to third generation leptons: DM coupling only to left-handed leptons ($y_R = 0$), DM coupling only to τ_R ($y_L = 0$), and DM with equal couplings to left- and right-handed leptons ($y_L = y_R$).

VI. SUMMARY

If dark matter is a Majorana fermion, its annihilation in the Sun to Standard Model fermions is both chirality and velocity-suppressed. Then, the annihilation may primarily be through 3-body processes, with the emission of a gauge boson. The neutrino spectra from such channels can differ dramatically from the spectra from $2 \rightarrow 2$ processes.

Dark matter couplings to left-handed leptons necessarily open-up 3-body annihilation channels in which neutrinos are produced directly. Moreover, the branching fractions to these channels are usually large. The neutrino injection spectra are typically hard, providing for interesting detection possibilities at neutrino detectors.

We considered a model in which $SU(2)$ -singlet DM couples to SM leptons (either left-handed or right-handed) via exchange of a new scalar $\eta_{L,R}$. For this model, we calculated the 3-body differential annihilation cross sections and the neutrino injection spectra with a full treatment of the helicity correlations of the gauge boson and τ lepton decays. We determined the muon event rates at IceCube/DeepCore arising from each annihilation channel, accounting for neutrino propagation effects, including oscillation, scattering and regeneration.

We calculated 3σ sensitivities of IC/DC to the DM-nucleon scattering cross section for several 3-body channels. The different channels are of varying utility in constraining dark matter models; channels with primary neutrinos lead to the best sensitivity.

We then showed how to combine the sensitivities in individual channels, to obtain the sensitivity for a combination of channels as may arise in models.

Acknowledgments. D.M. thanks the University of Hawaii for its hospitality during the initial stages of this work. J.K. and D.M. thank the Center for Theoretical Underground Physics and Related Areas (CETUP* 2012) in South Dakota for its support and hospitality during the completion of this work. This research was supported in part by DOE grants DE-FG02-04ER41291, DE-FG02-04ER41308 and DE-FG02-96ER40969, and by NSF grant PHY-0544278.

Appendix A: Vector boson emission cross sections

As shown in Ref. [6], the analytic form of the differential cross section is independent of the emitted electroweak gauge boson. Consequently, the set of differential and total cross sections for the various channels can be obtained from the following equations:

$$v_{rel} \frac{d\sigma}{dx_1 dx_2} \Big|_{XX \rightarrow f_L \bar{f}_L Z} = \frac{e^2 (1 - 2 \sin^2 \theta_W)^2 |y_L|^4 (4(x_1 + x_2 - 1) + \frac{m_z^2}{m_X^2}) \left(2(x_1^2 - 2x_1 + x_2^2 - 2x_2 + 2) - \frac{m_z^2}{m_X^2} \right)}{1024\pi^3 \sin^2 \theta_W \cos^2 \theta_W m_X^2 (1 - 2x_1 - r)^2 (1 - 2x_2 - r)^2},$$

$$\sigma_{XX \rightarrow f_R \bar{f}_R Z} = \frac{4 \sin^4 \theta_W}{(1 - 2 \sin^2 \theta_W)^2} \sigma_{XX \rightarrow f_L \bar{f}_L Z} \Big|_{y_L \rightarrow y_R}$$

$$\sigma_{XX \rightarrow \nu_L \bar{\nu}_L Z} = \frac{1}{(1 - 2 \sin^2 \theta_W)^2} \sigma_{XX \rightarrow f_L \bar{f}_L Z}$$

$$\sigma_{XX \rightarrow \nu_R \bar{\nu}_R Z} = 0$$

$$\sigma_{XX \rightarrow f_L \bar{\nu}_L W^+} = \sigma_{XX \rightarrow \bar{f}_L \nu_L W^-} = \frac{2 \cos^2 \theta_W}{(1 - 2 \sin^2 \theta_W)^2} \sigma_{XX \rightarrow f_L \bar{f}_L Z} \Big|_{m_Z \rightarrow m_W}$$

$$\sigma_{XX \rightarrow f_R \bar{\nu}_R W^+} = \sigma_{XX \rightarrow \bar{f}_R \nu_R W^-} = 0$$

$$\sigma_{XX \rightarrow f_L \bar{f}_L \gamma} = \frac{4 \sin^2 \theta_W \cos^2 \theta_W}{(1 - 2 \sin^2 \theta_W)^2} \sigma_{XX \rightarrow f_L \bar{f}_L Z} \Big|_{m_Z \rightarrow 0}$$

$$\sigma_{XX \rightarrow f_R \bar{f}_R \gamma} = \frac{\cos^2 \theta_W}{\sin^2 \theta_W} \sigma_{XX \rightarrow f_R \bar{f}_R Z} \Big|_{m_Z \rightarrow 0} = \sigma_{XX \rightarrow f_L \bar{f}_L \gamma} \Big|_{y_L \rightarrow y_R},$$

where [5]

$$v_{rel} \sigma_{XX \rightarrow f_L \bar{f}_L Z} = \frac{g^2 (1 - 2 \sin^2 \theta_W)^2 |y_L|^4}{1024\pi^3 \cos^2 \theta_W m_X^2} \left\{ (r+1) \left[\frac{\pi^2}{6} - \ln^2 \left(\frac{2m_X^2(r+1)}{4m_X^2 r - m_z^2} \right) - 2\text{Li}_2 \left(\frac{2m_X^2(r+1) - m_z^2}{4m_X^2 r - m_z^2} \right) \right. \right.$$

$$+ 2\text{Li}_2 \left(\frac{m_z^2}{2m_X^2(r+1)} \right) - \text{Li}_2 \left(\frac{m_z^2}{m_X^2(r+1)^2} \right) - 2\text{Li}_2 \left(\frac{m_z^2[r-1]}{2(m_X^2[r+1]^2 - m_z^2)} \right)$$

$$\left. + 2 \ln \left(\frac{4m_X^2 r - m_z^2}{2m_X^2(r-1)} \right) \ln \left(1 - \frac{m_z^2}{2m_X^2(r+1)} \right) + \ln \left(1 - \frac{m_z^2}{m_X^2(r+1)^2} \right) \ln \left(\frac{m_z^2(r-1)^2}{4(m_X^2(r+1)^2 - m_z^2)} \right) \right]$$

$$- \frac{m_z^2 (4m_X^2(r+1)(4r+3) - (r-3)(m_z^2 - 4m_X^2))}{16m_X^4(r+1)^2}$$

$$+ \frac{m_z^2 (m_z^4(-r-1) - 2m_z^2 m_X^2(r+1)(r+3) + 4m_X^4(r+1)^4)}{4m_X^4(r+1)^3 (m_X^2(r+1)^2 - m_z^2)} \ln \left(\frac{m_z^2}{4m_X^2} \right)$$

$$+ \frac{(r-1)(2m_X^2(r+1) - m_z^2) (-m_z^6 + 2m_z^4 m_X^2(r(r+4) + 1) - m_z^2 m_X^4(r+1)^2(3r(r+6) + 7) + 4m_X^6(r+1)^4(4r+1))}{4m_X^4(r+1)^3 (4m_X^2 r - m_z^2) (m_X^2(r+1)^2 - m_z^2)}$$

$$\left. \times \ln \left(\frac{2m_X^2(r-1)}{2m_X^2(r+1) - m_z^2} \right) + \frac{4r+3}{r+1} \right\}.$$

-
- [1] W. H. Press and D. N. Spergel, *Astrophys. J.* **296**, 679 (1985); K. Freese, *Phys. Lett. B* **167**, 295 (1986). L. M. Krauss, M. Srednicki and F. Wilczek, *Phys. Rev. D* **33**, 2079 (1986).
- [2] H. Goldberg, *Phys. Rev. Lett.* **50**, 1419 (1983) [Erratum-ibid. **103**, 099905 (2009)].
- [3] N. F. Bell, J. B. Dent, T. D. Jacques and T. J. Weiler, *Phys. Rev. D* **78**, 083540 (2008) [arXiv:0805.3423 [hep-ph]].
- [4] V. Barger, Y. Gao, W.-Y. Keung and D. Marfatia, *Phys. Rev. D* **80**, 063537 (2009) [arXiv:0906.3009 [hep-ph]].
- [5] N. F. Bell, J. B. Dent, A. J. Galea, T. D. Jacques, L. M. Krauss and T. J. Weiler, *Phys. Lett. B* **706**, 6 (2011) [arXiv:1104.3823 [hep-ph]].
- [6] V. Barger, W.-Y. Keung and D. Marfatia, *Phys. Lett. B* **707**, 385 (2012) [arXiv:1111.4523 [hep-ph]].
- [7] L. Bergstrom, T. Bringmann and J. Edsjo, *Phys. Rev. D* **78**, 103520 (2008) [arXiv:0808.3725 [astro-ph]].
- [8] M. Kachelriess, P. D. Serpico and M. Aa. Solberg, *Phys. Rev. D* **80**, 123533 (2009) [arXiv:0911.0001 [hep-ph]].
- [9] M. Garny, A. Ibarra and S. Vogl, *JCAP* **1107**, 028 (2011) [arXiv:1105.5367 [hep-ph]].
- [10] M. Garny, A. Ibarra and S. Vogl, *JCAP* **1204**, 033 (2012) [arXiv:1112.5155 [hep-ph]].
- [11] N. F. Bell, A. J. Brennan and T. D. Jacques, arXiv:1206.2977 [hep-ph].
- [12] E. Ma, *Phys. Rev. Lett.* **86**, 2502 (2001) [hep-ph/0011121].
- [13] K. Fukushima, J. Kumar and P. Sandick, *Phys. Rev. D* **84**, 014020 (2011) [arXiv:1103.5068 [hep-ph]].
- [14] P. Ciafaloni, M. Cirelli, D. Comelli, A. De Simone, A. Riotto and A. Urbano, *JCAP* **1106**, 018 (2011) [arXiv:1104.2996 [hep-ph]].
- [15] R. Mertig, M. Bohm and A. Denner, *Comput. Phys. Commun.* **64**, 345 (1991).
- [16] A. Pukhov, E. Boos, M. Dubinin, V. Edneral, V. Ilyin, D. Kovalenko, A. Kryukov and V. Savrin *et al.*, hep-ph/9908288. A. Pukhov, hep-ph/0412191.
- [17] V. Barger, Y. Gao and D. Marfatia, *Phys. Rev. D* **83**, 055012 (2011) [arXiv:1101.4410 [hep-ph]].
- [18] F. P. An *et al.* [Daya-Bay Collaboration], *Phys. Rev. Lett.* **108**, 171803 (2012) [arXiv:1203.1669 [hep-ex]].
- [19] V. Barger, J. Kumar, D. Marfatia and E. M. Sessolo, *Phys. Rev. D* **81**, 115010 (2010) [arXiv:1004.4573 [hep-ph]].
- [20] G. Jungman, M. Kamionkowski and K. Griest, *Phys. Rept.* **267**, 195 (1996) [hep-ph/9506380].
- [21] M. C. Gonzalez-Garcia, F. Halzen and S. Mohapatra, *Astropart. Phys.* **31**, 437 (2009) [arXiv:0902.1176 [astro-ph.HE]].
- [22] M. Honda, T. Kajita, K. Kasahara, S. Midorikawa and T. Sanuki, *Phys. Rev. D* **75**, 043006 (2007) [astro-ph/0611418].